

Magnetically Ordered State and Crystalline-Electric-Field Effects in SmBe₁₃

Hiroyuki Hidaka*, Seigo Yamazaki, Yusei Shimizu†, Naoyuki Miura, Chihiro Tabata‡, Tatsuya Yanagisawa, and Hiroshi Amitsuka

Graduate School of Science, Hokkaido University, Sapporo, Hokkaido 060-0810, Japan

The physical properties of single-crystalline SmBe₁₃ with a NaZn₁₃-type cubic structure have been studied by electrical resistivity (ρ), specific heat (C), and magnetization (M) measurements in magnetic fields of up to 9 T. The temperature (T) dependence of ρ shows normal metallic behavior without showing the Kondo – $\ln T$ behavior, suggesting the weak hybridization effect in this system. Analyses of the temperature dependence of C suggest that the Sm ions of this compound are trivalent and that the crystalline-electric-field (CEF) ground state is a Γ_8 quartet with a first-excited state of a Γ_7 doublet located at the energy scale of ~ 90 K. Mean-field calculations based on the suggested CEF level scheme can reasonably well reproduce the T dependence of magnetic susceptibility (χ) below ~ 70 K. These results in the paramagnetic state strongly indicate that the $4f$ electrons are well localized with the Sm³⁺ configuration. At low temperatures, the $4f$ electrons undergo a magnetic order at $T_M \sim 8.3$ K, where $\chi(T)$ shows an antiferromagnetic-like cusp anomaly. From the positive Curie–Weiss temperature obtained from the mean-field calculations and from a constructed magnetic phase diagram with multiple regions, we discussed the magnetic structure of SmBe₁₃ below T_M , by comparing with other isostructural MBe₁₃ compounds showing helical-magnetic ordering.

1. Introduction

The intermetallic compounds MBe₁₃ (M = rare earths and actinides) have attracted much interest because of the rich variety of their physical properties, such as unconventional superconductivity (SC) in UBe₁₃,¹⁾ an intermediate-valence state in CeBe₁₃,²⁾ helical-magnetic ordering in HoBe₁₃,³⁾ and nuclear-antiferromagnetic (AFM) ordering in PrBe₁₃.⁴⁾ Among them, UBe₁₃ is well known as a heavy-fermion (HF) superconductor with an extremely large electric specific-heat coefficient γ (~ 1.1 J K⁻² mol⁻¹).¹⁾ A number of studies have been conducted in order to reveal the still undetermined origin of the unconventional SC and its non-Fermi-liquid behavior in the normal phase of UBe₁₃ for more than thirty years.⁵⁾ To obtain further insights into the novel features of UBe₁₃, it will be useful to reveal the common properties and differences in a series of isostructural MBe₁₃ compounds by studying the ground-state properties as well as magnetic correlations for each compound in more detail.

The MBe₁₃ compounds crystallize in a NaZn₁₃-type cubic structure with the space group $Fm\bar{3}c$ (No. 226, O_h^6), where the unit cell contains M atoms in the $8a$ site, Be^I atoms in the $8b$ site, and Be^{II} atoms in the $96i$ site.^{6–8)} It is characteristic that the unit cell consists of two cagelike structures: the M atom is surrounded by 24 Be^{II} atoms, nearly forming a snub cube, and the Be^I atom is surrounded by 12 Be^{II} atoms, forming an icosahedron cage. Recent studies of the strongly correlated electron systems with cagelike structures (e.g., filled skutterudites) have revealed that these systems are expected to commonly have the following characteristics: higher-order multipole degrees of freedom, strong c - f hybridization, and low-energy phonon modes associated with the local vibration

of a guest atom with a large amplitude in an oversized host cage, called rattling.^{9–11)} They have provided new hot topics in strongly correlated electron physics.

The MBe₁₃ systems also exhibit these characteristics, which possibly originated from the cagelike structure; CeBe₁₃ is known as an intermediate-valence compound due to the strong c - f hybridization,^{2,12)} and LaBe₁₃, UBe₁₃, and ThBe₁₃ have been reported to possess a low-energy phonon mode associated with the presence of a low-energy Einstein phonon mode with characteristic temperatures (θ_E) of ~ 177 , 151, and 157 K, respectively.^{13–15)} In this study, we focus our attention on SmBe₁₃. Sm-based compounds have been attracting much interest because of their valence-fluctuation behavior.^{16,17)} In addition, novel phenomena have recently been found in cage-structural Sm-based compounds with cubic symmetry, such as an unusually field-insensitive HF state in SmOs₄Sb₁₂¹⁸⁾ and a magnetic-octupole ordering in SmRu₄P₁₂.^{19,20)} It is thus intriguing to investigate the behavior of the Sm ions that are placed in the cage-structural environment.

For SmBe₁₃, there have been only two reports on polycrystalline samples so far.^{6,21)} These previous works revealed the presence of a phase transition at 8.8 K, and proposed a crystalline-electric-field (CEF) level scheme for the $4f$ electrons of Sm with a Γ_7 doublet ground state and a Γ_8 quartet first-excited state located at 12.5⁶⁾ or 30 K.²¹⁾ However, the origin of the phase transition has not yet been clarified, and no attempt to grow a single crystal has been reported. Recently, we have succeeded in growing single crystals of SmBe₁₃, and we performed ultrasonic measurements under high magnetic fields, which revealed the Γ_8 ground state rather than the Γ_7 ground state.²²⁾ In addition, recent Mössbauer spectroscopy measurements revealed the trivalent state of the Sm ions at room temperature.²³⁾ In this paper, we report the results of electrical resistivity (ρ), specific heat (C), and magnetization (M) measurements on single-crystalline SmBe₁₃.

*E-mail: hidaka@phys.sci.hokudai.ac.jp

†Present address: Institute for Materials Research, Tohoku University, Oarai, Ibaraki 311-1313, Japan

‡Present address: Condensed Matter Research Center and Photon Factory, Institute of Materials Structure Science, High Energy Accelerator Research Organization, Tsukuba, Ibaraki 305-0801, Japan

2. Experimental Procedure

Two batches of single crystals of SmBe_{13} , which are labeled “#1” and “#2”, were grown by the Al-flux method. The constituent materials (Sm with 99.9% purity and Be with 99% purity) and Al with 99.99% purity were placed in an Al_2O_3 crucible at an atomic ratio of 1:13:30 and sealed in a quartz tube filled with ultrahigh-purity Ar gas of ~ 150 mmHg. The sealed tube was kept at 1050 °C for 1 week and then cooled at a rate of 2 °C/h. The Al flux was spun off in a centrifuge and then removed by NaOH solution. The obtained single crystals were annealed for 2 weeks at 700 °C. The typical size of a grown sample is about $1 \times 1 \times 1$ mm³. The results of powder X-ray diffraction (XRD) at room temperature showed no impurity phase. The lattice parameter of SmBe_{13} was obtained to be $a = 10.313$ Å, which is close to the previously reported value of $a = 10.304$ Å.⁶ In the recent single-crystal XRD measurements performed by our collaborators using synchrotron X-rays, the full width at half maximum of a rocking curve of the (200) reflection was estimated to be approximately 0.1° , indicating the low mosaicity of the single crystals prepared in this study.

Electrical resistivity measurements using a crystal piece taken from batch #1 were performed by a conventional four-probe method in the temperature range of $0.1 - 300$ K with a $^3\text{He}/^4\text{He}$ dilution refrigerator. The electrical current j was applied in the [100] direction. Specific heat measurements were performed using a crystal piece taken from batch #2 by a thermal-relaxation method in the magnetic-field range of $0 - 9$ T and in the temperature range of $2 - 300$ K with a Physical Property Measurement System (PPMS, Quantum Design, Inc.). DC magnetization measurements were performed using the piece taken from batch #2 in magnetic fields of up to 7 T and in the temperature range from 2 to 370 K by a Magnetic Property Measurement System (MPMS, Quantum Design, Inc.). The weight of the sample used for the specific heat and magnetization measurements was ~ 9.6 mg.

3. Experimental Results

3.1 Electrical resistivity

Figure 1 shows the temperature dependence of the electrical resistivity $\rho(T)$ of SmBe_{13} for annealed and as-grown samples (batch #1). By annealing the sample, the residual resistivity ratio (RRR) increases from 5 to 9, and the residual resistivity decreases from 7.1 to 2.7 $\mu\Omega\text{cm}$. In both the annealed and as-grown samples, $\rho(T)$ exhibits typical metallic behavior without any increase in ρ with decreasing temperature associated with the Kondo effect, i.e., $-\ln T$ behavior, in the whole T range. This suggests that the c - f hybridization effect is weak in this compound.

At low temperatures, the $\rho(T)$ curve shows a kink anomaly due to a phase transition at T_M , as shown in the inset of Fig. 1. The kink anomaly for the annealed sample is sharper and more obvious than that for the as-grown one. Here, the transition temperature T_M was defined as the temperature at which $-\text{d}^2\rho/\text{d}T^2$ takes the maximum value. The obtained transition temperature T_M for the annealed sample (~ 8.7 K) is higher than that for the as-grown one (~ 6.5 K) and in good agreement with that reported previously (~ 8.8 K).⁶

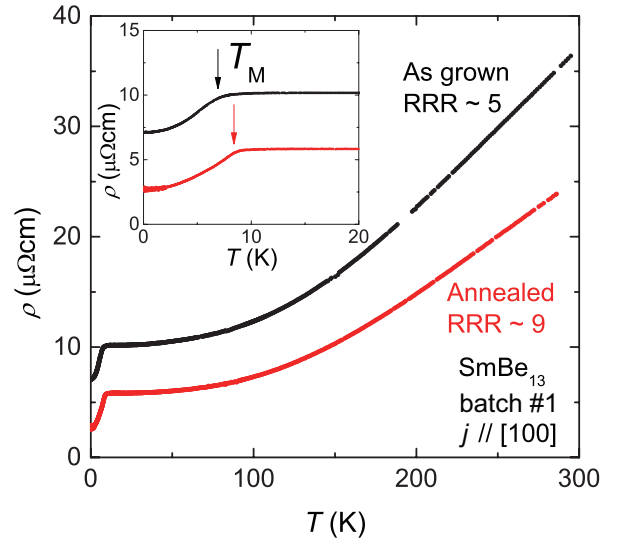


Fig. 1. (Color online) Temperature dependence of electrical resistivity $\rho(T)$ of SmBe_{13} for the annealed (red) and as-grown (black) samples from batch #1. The inset shows the enlarged view below 20 K. The arrows indicate the transition temperature T_M .

3.2 Specific heat

Figure 2 shows the temperature dependence of the specific heat divided by the temperature $C(T)/T$ for the annealed SmBe_{13} (batch #2) and LaBe_{13} .¹³ The $C(T)/T$ curve of LaBe_{13} obeys the Debye T^3 law below ~ 10 K, where γ and the Debye temperature θ_D were estimated to be ~ 9.1 mJ K⁻² mol⁻¹ and ~ 950 K, respectively.¹³ Furthermore, the $C(T)/T$ curve for LaBe_{13} shows a broad hump at around 40 K, which can be well described by a simple model assuming a low-energy Einstein phonon mode with θ_E of ~ 177 K.¹³ Note that the $C(T)/T$ curve of SmBe_{13} also has a similar hump structure near 40 K, which should involve the CEF Schottky contribution as well as the low-energy Einstein phonon contribution, as discussed below. Here, the value of C/T for SmBe_{13} is slightly smaller than that for LaBe_{13} above ~ 80 K, which may be due to the difference in the phonon contributions.

The $C(T)/T$ curve of SmBe_{13} exhibits a λ -type anomaly at $T_M = 8.3$ K, indicating that a second-order phase transition takes place at this temperature. The T_M determined from the C measurements is slightly lower than that obtained from the present ρ measurements, which may originate from the difference in the measured sample batches. Below T_M , a shoulder structure can be seen in $C(T)/T$ (see the inset of Fig. 2), suggesting that the ordering cannot be described by a simple mean-field model with a doublet CEF ground state. The inset also displays $C(T)/T$ near T_M in magnetic fields applied in the [100] direction. T_M shifts to the low-temperature side with increasing magnetic field.

Next, we estimated the contribution of $4f$ electrons to the specific heat (C_{4f}) for SmBe_{13} by subtracting $C(T)$ of LaBe_{13} from that of SmBe_{13} , as shown in Fig. 3. The $4f$ -electron entropy $\Delta S_{4f} [\equiv S_{4f}(T) - S_{4f}(2 \text{ K})]$ was obtained by integrating $C_{4f}(T)/T$ from 2 K. In the cubic CEF with the O_h symmetry, the $J = 5/2$ ground multiplet of Sm^{3+} splits into a Γ_8 quartet and a Γ_7 doublet. In SmBe_{13} , the Γ_8 quartet should be the CEF ground state since ΔS_{4f} reaches $0.73R\ln 4$ at T_M , which is significantly larger than $R\ln 2$. This is consistent with the sug-

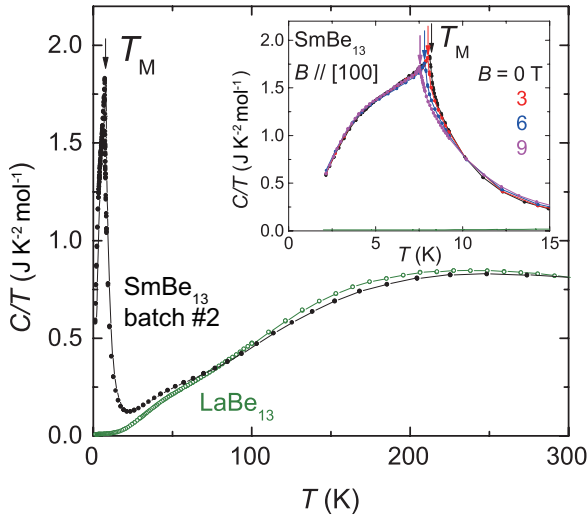


Fig. 2. (Color online) Temperature dependence of C/T for SmBe_{13} (closed circles) and LaBe_{13} (open circles)¹³⁾ below 300 K at zero field. The inset shows the temperature dependence of C/T below 15 K in various magnetic fields applied in the [100] direction. The arrows represent T_M determined from the peak in $C(T)/T$ at each magnetic field.

gested CEF ground state from the previous ultrasonic measurements.²²⁾ Note that the actual $4f$ -electron entropy at T_M must be even closer to $R\ln 4$ than $\Delta S_{4f}(T_M)$ estimated above 2 K. The reduction in ΔS_{4f} from $R\ln 4$ at T_M is considered to be due to the occurrence of a short-range ordering above T_M , since the effect of the c - f hybridization is considered to be negligibly small, as suggested from the absence of $-\ln T$ behavior in $\rho(T)$.

At higher temperatures ($T \sim 80$ K), $\Delta S_{4f}(T)$ reaches approximately $R\ln 6$, which is the expected value in the $J = 5/2$ multiplet state, suggesting that the Sm ions are trivalent. The trivalent state of the Sm ions for SmBe_{13} has also been confirmed by Mössbauer spectroscopy at room temperature.²³⁾ A broad maximum of the $C_{4f}(T)$ curve at around 40 K is mainly attributed to the CEF Schottky anomaly. Here, the phonon contribution at low temperatures in SmBe_{13} is considered to be approximated by that in LaBe_{13} , since θ_E estimated from our recent XRD studies does not show an obvious difference between LaBe_{13} [θ_E of 163(15) K] and SmBe_{13} [θ_E of 157(10) K].²⁴⁾ Assuming a $\Gamma_8 - \Gamma_7$ level scheme with energy separation Δ_{CEF} of 90 K, the broad maximum can be reproduced well by the calculated CEF Schottky curve in this work (the red dot-dashed line in Fig. 3). For the sake of comparison, we also represented the calculated $C_{4f}(T)$ curves based on the previously reported CEF level schemes: the $\Gamma_7 - \Gamma_8$ model with $\Delta_{\text{CEF}} = 12.5$ K determined from the C measurements by Bucher et al.,⁶⁾ and the $\Gamma_7 - \Gamma_8$ model with $\Delta_{\text{CEF}} = 30$ K determined from the M measurements by Besnus et al.²¹⁾ Both of them, however, cannot explain the broad maximum in $C_{4f}(T)$ at ~ 40 K.

3.3 Magnetic susceptibility and magnetization curve

The temperature dependence of the magnetic susceptibility $\chi(T) [= M(T)/B]$ of SmBe_{13} measured at $B = 0.1$ T between 2 and 370 K is shown in Fig. 4. The measured sample was an annealed single crystal taken from batch #2, and the magnetic field was applied along the [100] axis. $\chi(T)$ is nearly

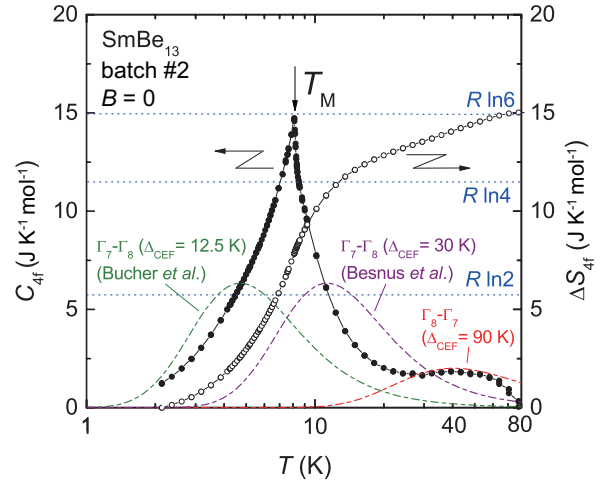


Fig. 3. (Color online) Temperature dependences of C_{4f} and ΔS_{4f} in SmBe_{13} at zero magnetic field, where $\Delta S_{4f} \equiv S_{4f}(T) - S_{4f}(2 \text{ K})$. The red, green, and purple dot-dashed lines represent the calculated CEF Schottky curves proposed by this study, Bucher et al.,⁶⁾ and Besnus et al.,²¹⁾ respectively.

constant at high temperatures and starts increasing gradually with decreasing temperature below ~ 300 K. Such behavior has also been reported in other Sm-based compounds, such as SmAl_2 ²⁵⁾ and $\text{SmTi}_2\text{Al}_{20}$,²⁶⁾ where this behavior has been interpreted to be due to the mixing of the low-lying $J = 7/2$ excited multiplet of Sm^{3+} into the $J = 5/2$ ground multiplet. The increase in $\chi(T)$ for SmBe_{13} becomes more pronounced below ~ 100 K. The experimental data between 15 and 70 K can be reasonably well described in terms of the following mean-field model:

$$\chi(T) = \frac{\chi_{\text{CEF}}(T)}{1 - \lambda \chi_{\text{CEF}}(T)} + \chi_0, \quad (1)$$

where λ is the mean-field constant:

$$\lambda = \frac{3k_B \theta_{\text{CW}}}{N_A \mu_B^2 g_J^2 J(J+1)}, \quad (2)$$

χ_{CEF} is the single-ion magnetic susceptibility assuming the $\Gamma_8 - \Gamma_7$ CEF level scheme of the $J = 5/2$ multiplet for Sm^{3+} with $\Delta_{\text{CEF}} = 90$ K, χ_0 is a constant, k_B is the Boltzmann constant, θ_{CW} is the Curie–Weiss temperature, N_A is Avogadro's number, μ_B is the Bohr magneton, $g_J = 2/7$ is the Landé g factor, and $J = 5/2$. From the best fit, we obtained χ_0 to be 3.2×10^{-4} emu/mol and θ_{CW} to be 10.8 K. The good agreement between the experimental data and the mean-field calculation suggests that the magnetic-dipole moments of the $4f$ electrons are hardly reduced below 70 K. The $\chi(T)$ curve deviates from the fitting curve below ~ 15 K, probably due to the short-range ordering, and then it exhibits a clear cusp at $T_M = 8.3$ K. It is noteworthy that such a cusp anomaly is associated with the occurrence of AFM ordering, despite the fact that the obtained value of θ_{CW} ($= 10.8$ K) is positive, indicating that the total effective magnetic interaction between the Sm $4f$ moments is ferromagnetic (FM).

Figure 5 shows the temperature dependence of the magnetization $M(T)$ at various magnetic fields up to 7 T. The magnetic field was applied in the [100] direction. At each magnetic field, the results of zero-field-cooling (ZFC) and field-cooling (FC) processes are shown in Fig. 5. The $M(T)$ curves

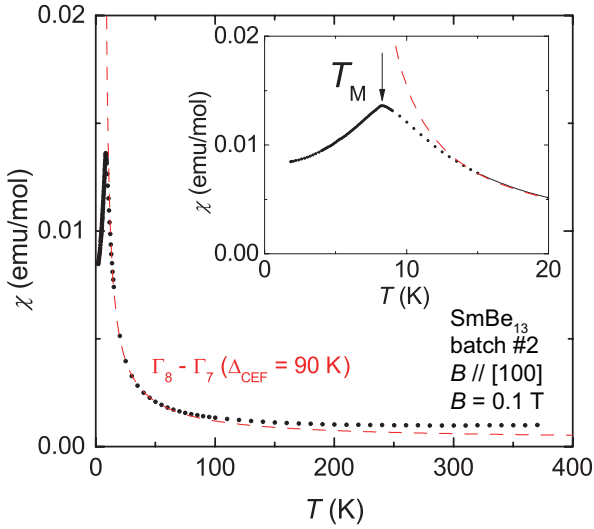


Fig. 4. (Color online) Temperature dependence of magnetic susceptibility $\chi(T)$ in SmBe_{13} at $B = 0.1$ T for $B // [100]$. The inset shows $\chi(T)$ below 20 K. The red-dashed line represents the fitting curve obtained from the mean-field calculation, as described in the text.

at low magnetic fields show a cusp anomaly at T_M . However, the decrease in M below T_M is gradually suppressed with increasing magnetic field, and then the cusp anomaly at T_M becomes a kink anomaly above 5 T. Here, we determined T_M from the temperature where d^2M/dT^2 shows a local minimum. T_M slightly decreases with increasing field, in good agreement with the results obtained from the present C measurements. In addition to the T_M anomaly, the ZFC curves above 3 T show another kink anomaly at a lower temperature than T_M , defined as T_X . T_X decreases linearly with increasing magnetic field, where T_X was also determined from the local minimum position of d^2M/dT^2 . Moreover, there is a significant difference in $M(T)$ between the ZFC and FC curves below $\sim T_X$, suggesting the possible presence of magnetic domains.

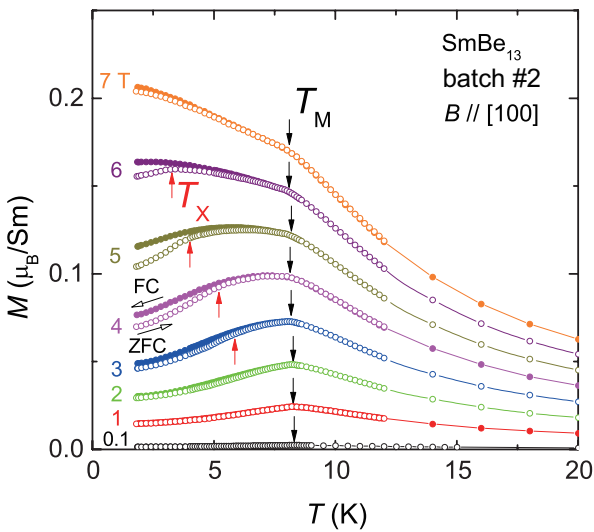


Fig. 5. (Color online) Temperature dependence of magnetization for SmBe_{13} measured at various magnetic fields from 0.1 to 7 T. The open and closed symbols represent the data obtained from the ZFC and FC processes, respectively. The black and red arrows indicate T_M and T_X , respectively.

Figure 6 shows the magnetization curves $M(B)$ of SmBe_{13} , measured at various temperatures between 2 and 12 K for fields up to 7 T parallel to $[100]$. $M(B)$ at 12 K (above T_M) exhibits simple paramagnetic (PM) behavior with a Brillouin curve. On the other hand, below T_M , the $M(B)$ curves bend upward at the newly defined characteristic field B_X . Here, we determined B_X from the intersection of two linear extrapolations from the higher- and lower-field regions. With decreasing temperature, the bending becomes distinct and B_X shifts to the higher-field side. At the lowest temperature of 2 K, B_X reaches approximately 4 T.

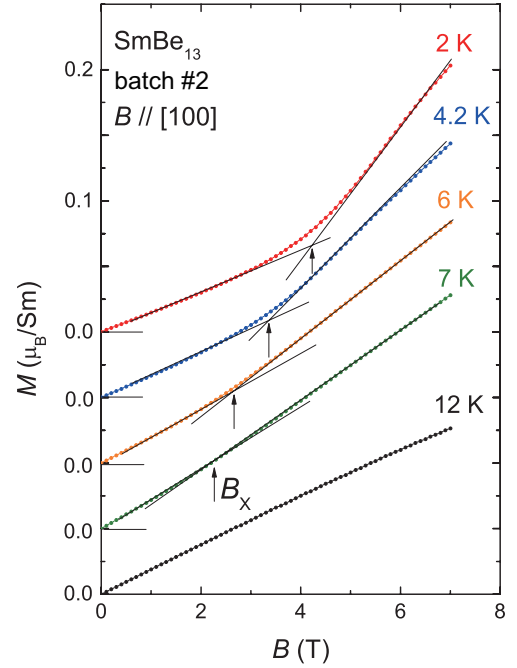


Fig. 6. (Color online) Magnetization of SmBe_{13} up to 7 T ($B // [100]$) at several temperatures ($T = 2, 4.2, 6, 7,$ and 12 K). All the solid lines are guides to the eye, and the arrows indicate the intersection of two linear extrapolations, giving the definition of B_X .

3.4 Magnetic phase diagram

The magnetic field–temperature (B – T) phase diagram of SmBe_{13} for $B // [100]$, constructed from the C (closed symbols) and M (open symbols) measurements, is shown in Fig. 7. As the magnetic field increases to 9 T, T_M decreases from 8.3 to 7.7 K. The most striking feature is that the B – T phase diagram of SmBe_{13} consists of three regions below T_M , indicating that the magnetic structure of this compound changes with the applied magnetic field. Here, we refer to these three regions as I, II, and III (see Fig. 7). Figure 7 also shows a contour plot of the difference in $M(T)$ between the ZFC and FC processes ($\equiv \Delta M$), where the red color represents the largest ΔM . This contour plot revealed that ΔM is present only in region III. Note that this magnetic phase diagram, including the difference between the ZFC and FC processes below T_X , is consistent with that obtained from ultrasonic measurements under magnetic fields.²²⁾

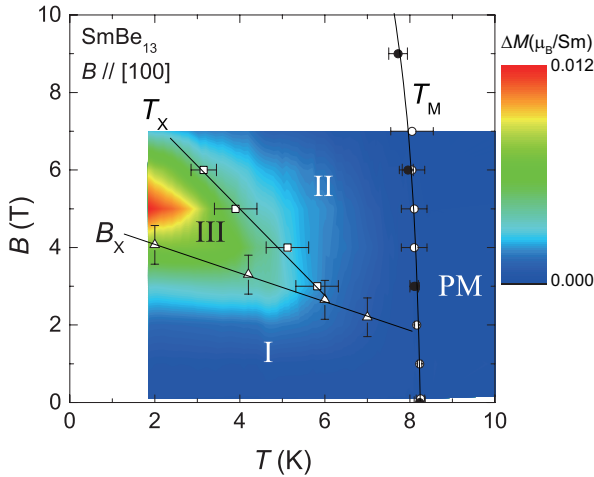


Fig. 7. (Color online) B - T phase diagram of SmBe_{13} for $B \parallel [100]$ axis. There are three regions (named I, II, and III) below T_M . The solid lines are guides to the eye. In this figure, a contour plot of ΔM is also shown simultaneously.

4. Discussion

We now discuss a possible ordering state of SmBe_{13} . Recently, novel orderings, which show an unusual magnetic-field response, have been found in some cage-structural Sm-based compounds; for example, the ordering temperature for $\text{SmRu}_4\text{P}_{12}$ increases with increasing magnetic field,²⁷⁾ while $\text{SmTr}_2\text{Al}_{20}$ (Tr = Ti and Ta) show a rather magnetic-field-insensitive phase transition.^{26,28)} These behaviors are considered to be related to magnetic-octupole degrees of freedom in the Γ_8 quartet ground state.^{19,26,28)} SmBe_{13} also has the cage-like structure and the Γ_8 ground state; nevertheless such unusual field dependence of T_M cannot be observed.²²⁾ In addition, our recent muon-spin relaxation measurements of SmBe_{13} indicate that an internal magnetic field larger than 0.1 T occurs at a muon stopping site below T_M ,²⁹⁾ suggesting that the primary order parameter for SmBe_{13} is a magnetic dipole. Thus, the simplest explanation for the ordering state of SmBe_{13} is an AFM ordering, since the $\chi(T)$ curve shows the cusp anomaly at T_M , and T_M decreases by applying a magnetic field. However, the occurrence of the simple AFM ordering appears to contradict the presence of the dominant FM interaction in the PM state, suggesting that the ordered state of SmBe_{13} has a rather complex magnetic structure. High-field ultrasonic measurements up to 61.3 T revealed that the ordered state of SmBe_{13} is suppressed by a magnetic field of 43 T for $B \parallel [100]$ axis.²²⁾ The obtained critical magnetic field deviates from the value estimated from the mean-field calculation assuming the Γ_8 CEF ground state and a simple G-type AFM state.²²⁾

We suggest that the most plausible candidate for the ordered state of SmBe_{13} is a helical-magnetic ordering. It is noteworthy that many MBe_{13} compounds with $M = \text{Gd} - \text{Er}$ and Np order into a helical-magnetic structure with propagation vector $\mathbf{Q} \sim [00\frac{1}{3}]$ at the transition temperature T_{heli} .^{3,30)} They also show both an AFM-like cusp anomaly at T_{heli} in $\chi(T)$ and a positive θ_{CW} , whose absolute value is comparable to T_{heli} . These features are similar to those in SmBe_{13} . In the heavy-rare-earth MBe_{13} compounds, the occurrence of the helical ordering is explained by competition between exchange

interactions between the first- and second-neighboring (100) planes, where each plane has a strong FM interaction.³¹⁾ Here, we defined the c -axis as the helical axis of the magnetic structure in a cubic crystal for convenience. In this model, the exchange interactions between the first- and second-neighboring c planes were assumed to be FM and AFM, respectively. Since these MBe_{13} compounds are metallic systems with well-localized f electrons,^{6,32)} their magnetic interactions are considered to originate from the Ruderman-Kittel-Kasuya-Yosida (RKKY) interaction. In this context, the competition between the exchange interactions may be due to the oscillation of spin polarization, namely, the RKKY oscillation.

In addition, the magnetic phase diagram of SmBe_{13} constructed from this study is similar to that reported previously for the helical magnet HoBe_{13} .³²⁾ In this system, neutron diffraction measurements have revealed that two magnetic transitions are successively induced below T_{heli} by applying a magnetic field along the c -axis; the first one is from the helical structure with three domains to a single-domain conical structure, and the second one is from the conical structure to a two-domain canted magnetic structure.³²⁾ If SmBe_{13} has similar magnetic structures below T_M , the multiple regions in the phase diagram can be understood. The change in slope of the $M(B)$ curve and the finite ΔM in region III of SmBe_{13} could be explained by the presence of the spontaneous FM component derived from the conical structure with magnetic domains. Such a difference in $M(T)$ between the FC and ZFC processes has also been observed in a conical-ordered phase of Pd_3Mn .³³⁾ However, since these suggestions are based solely on the results of M measurements, we should not exclude the possibility of other magnetic structures accompanying the spontaneous FM components, for instance, a fan structure, canted AFM structure, and uncompensated AFM structure. Furthermore, the $M(B)$ curve of SmBe_{13} does not show a metamagnetic transition near the region boundary, which is different from the cases of HoBe_{13} and the typical helical magnet MnP .³⁴⁾ To clarify the magnetic structures below T_M of SmBe_{13} , we need further detailed studies, particularly microscopic measurements, such as neutron scattering on isotope-substituted samples and nuclear magnetic resonance.

If SmBe_{13} also exhibits the helical-magnetic ordering at T_M , it will be the first collateral evidence that the helical-ordering state is a common ground state in the magnetic MBe_{13} compounds including the light-rare-earth systems. Note that the ground state of UBe_{13} is not the helical ordering but the unconventional SC. In addition, the inelastic neutron scattering measurements for UBe_{13} have revealed the development of AFM short-range magnetic correlations with the propagation vector $\mathbf{q} = [\frac{1}{2}\frac{1}{2}0]$ at low temperatures.³⁵⁾ It is necessary to elucidate the reason why only UBe_{13} possesses a different ground state and magnetic correlation from those in other magnetic MBe_{13} compounds.

5. Summary

We have succeeded in growing single crystals of SmBe_{13} , and we reported the results of C , M , and ρ measurements using the grown single crystals. From this study, we obtained the following results concerning a PM state: (i) $4f$ electrons of Sm^{3+} ions are well localized, (ii) a plausible CEF level scheme is $\Gamma_8 - \Gamma_7$ ($\Delta_{\text{CEF}} = 90$ K), and (iii) the dominant

magnetic interaction between the $4f$ -dipole moments is FM on the whole. Interestingly, $\chi(T)$ shows an AFM-like cusp anomaly at $T_M \sim 8.3$ K despite the presence of the dominant FM interaction ($\theta_{CW} \sim 10.8$ K). Similar features have also been found in other isostructural MBe₁₃ compounds showing helical-magnetic ordering. Furthermore, a magnetic phase diagram with multiple regions of SmBe₁₃ was constructed from the C and M measurements under a magnetic field. The obtained phase diagram seems to be similar to that of the isostructural system HoBe₁₃, which shows the helical ordering. These findings suggest that SmBe₁₃ undergoes a helical or similar magnetic ordering at T_M .

The present research was supported by JSPS KAKENHI Grant Numbers JP20224015(S), JP25400346(C), JP26400342(C), JP15H05882, and JP15H05885(J-Physics).

- 1) H. R. Ott, H. Rudigier, Z. Fisk, and J. L. Smith, Phys. Rev. Lett. **50**, 1595 (1983).
- 2) Z. S. Wilson, R. T. Macaluso, E. D. Bauer, J. L. Smith, J. D. Thompson, Z. Fisk, G. G. Stanley, and J. Y. Chan, J. Am. Chem. Soc. **126**, 13926 (2004).
- 3) F. Bourée-Vigeneron, Phys. Scr. **44**, 27 (1991).
- 4) P. L. Moyland, T. Lang, E. D. Adams, G. R. Stewart, and Y. Takano, Czech. J. Phys. **46**, Suppl. S4, 2199 (1996).
- 5) For experimental reviews, see, for example, C. Pfleiderer, Rev. Mod. Phys. **81**, 1551 (2009).
- 6) E. Bucher, J. P. Maita, G. W. Hull, R. C. Fulton, and A. S. Cooper, Phys. Rev. B **11**, 440 (1975).
- 7) M. W. McElfresh, J. H. Hall, R. R. Ryan, J. L. Smith, and Z. Fisk, Acta Crystallogr. C **46**, 1579 (1990).
- 8) K. Takegahara, H. Harima, and T. Kasuya, J. Phys. F: Met. Phys. **16**, 1691 (1986).
- 9) Y. Aoki, H. Sugawara, H. Harima, and H. Sato, J. Phys. Soc. Jpn. **74**, 209 (2005).
- 10) T. Onimaru, K. T. Matsumoto, Y. F. Inoue, K. Umeo, T. Sakakibara, Y. Karaki, M. Kubota, and T. Takabatake, Phys. Rev. Lett. **106**, 177001 (2011).
- 11) T. Yanagisawa, Y. Ikeda, H. Saito, H. Hidaka, H. Amitsuka, K. Araki, M. Akatsu, Y. Nemoto, T. Goto, P. -C. Ho, R. E. Baumbach, and M. B. Maple, J. Phys. Soc. Jpn. **80**, 043601 (2011).
- 12) J. M. Lawrence, A. J. Arko, J. J. Joyce, R. I. R. Blyth, R. J. Bartlett, P. C. Canfield, and Z. Fisk, and P. S. Riseborough, Phys. Rev. B **47**, 15460 (1993).
- 13) H. Hidaka, Y. Shimizu, S. Yamazaki, N. Miura, R. Nagata, C. Tabata, S. Mombetsu, T. Yanagisawa, and H. Amitsuka, J. Phys. Soc. Jpn. **86**, 043601 (2017).
- 14) B. Renker, F. Gompf, W. Reichardt, H. Rietschel, J. B. Suck, and J. Beuers, Phys. Rev. B **32**, 1859 (1985).
- 15) R. Felten, F. Steglich, G. Weber, H. Rietschel, F. Gompf, B. Renker, and J. Beuers, Europhys. Lett. **2**, 321 (1986).
- 16) M. B. Maple and D. Wohlleben, Phys. Rev. Lett. **27**, 511 (1971).
- 17) A. Menth, E. Buehler, and T. H. Geballe, Phys. Rev. Lett. **22**, 295 (1969).
- 18) S. Sanada, Y. Aoki, H. Aoki, A. Tsuchiya, D. Kikuchi, H. Sugawara, and H. Sato, J. Phys. Soc. Jpn. **74**, 246 (2005).
- 19) M. Yoshizawa, Y. Nakanishi, M. Oikawa, C. Sekine, I. Shirotni, S. R. Saha, H. Sugawara, and H. Sato, J. Phys. Soc. Jpn. **74**, 2141 (2005).
- 20) Y. Aoki, S. Sanada, D. Kikuchi, H. Sugawara, and H. Sato, J. Phys. Soc. Jpn. **76**, 113703 (2007).
- 21) M. J. Besnus, P. Panissod, J. P. Kappler, G. Heinrich, and A. Meyer, J. Magn. Magn. Mater. **31–34**, 227 (1983).
- 22) S. Mombetsu, T. Murazumi, K. Hiura, S. Yamazaki, Y. Shimizu, H. Hidaka, T. Yanagisawa, H. Amitsuka, S. Yasin, S. Zherlitsyn, and J. Wosnitza, J. Phys. Conf. Ser. **683**, 012032 (2016).
- 23) S. Tsutsui, R. Masuda, Y. Kobayashi, Y. Yoda, K. Mizuuchi, Y. Shimizu, H. Hidaka, T. Yanagisawa, H. Amitsuka, F. Iga, and M. Seto, J. Phys. Soc. Jpn. **85**, 083704 (2016).
- 24) H. Hidaka, R. Nagata, C. Tabata, Y. Shimizu, N. Miura, T. Yanagisawa, and H. Amitsuka, in preparation for submission.
- 25) H. W. de Wijn, A. M. van Diepen, and K. H. J. Buschow, Phys. Rev. B **7**, 524 (1973).
- 26) R. Higashinaka, T. Maruyama, A. Nakama, R. Miyazaki, Y. Aoki, and H. Sato, J. Phys. Soc. Jpn. **80**, 093703 (2011).
- 27) K. Matsuhira, Y. Hinatsu, C. Sekine, T. Togashi, H. Maki, I. Shirotni, H. Kitazawa, T. Takamasu, and G. Kido, J. Phys. Soc. Jpn. **71**, Suppl. 237 (2002).
- 28) A. Yamada, R. Higashinaka, R. Miyazaki, K. Fushiya, T. D. Matsuda, Y. Aoki, W. Fujita, H. Harima, and H. Sato, J. Phys. Soc. Jpn. **82**, 123710 (2013).
- 29) C. Tabata, S. Yamazaki, T. U. Ito, W. Higemoto, N. Miura, Y. Shimizu, H. Hidaka, T. Yanagisawa, and H. Amitsuka, in preparation for submission.
- 30) A. Hiess, M. Bonnet, P. Burlet, E. Ressouche, J.-P. Sanchez, J. C. Waerenborgh, S. Zwirner, F. Wastin, J. Rebizant, G. H. Lander, and J. L. Smith, Phys. Rev. Lett. **77**, 3917 (1996).
- 31) P. J. Becker, M. Bonnet, and F. Vigneron, Mol. Cryst. Liq. Cryst. **125**, 405 (1985).
- 32) P. Dervnagas, P. Burlet, M. Bonnet, F. Bourdarot, A. Hiess, S. L. Bud'ko, P. C. Canfield, G. H. Lander, J. S. Kim, and G. R. Stewart, Phys. Rev. B **61**, 405 (2000).
- 33) P. Önnerud, Y. Andersson, and R. Tellgren, J. Solid State Chem. **128**, 109 (1997).
- 34) T. Komatsubara, T. Suzuki, and E. Hirahara, J. Phys. Soc. Jpn. **28**, 317 (1970).
- 35) S. Coad, A. Hiess, D. F. McMorro, G. H. Lander, G. Aeppli, Z. Fisk, G. R. Stewart, S. M. Hayden, and H. A. Mook, Physica B **276-278**, 764 (2000).